frontiers in Energy Research

ORIGINAL RESEARCH
published: 25 August 2021
doi: 10.3389/fenrg.2021.710907

Formation of Bubble-Loop Complexes During Helium Radiation in Fe-9Cr Steel

*Tiantian Shi[1], Wenbo Liu[1], Zhengxiong Su[1], Xu Yan[1], Chenyang Lu[1], Zhaoxi Yang[1], Xinfu He[2], Wei Yan[3] and Di Yun[1,4]**

[1]Department of Nuclear Science and Technology, Xi'an Jiaotong University, Xi'an, China, [2]Reactor Engineering Technology Research Division, China Institute of Atomic Energy, Beijing, China, [3]Shi-changxu Innovation Center for Advanced Materials, Institute of Metal Research, Chinese Academy of Sciences, Shenyang, China, [4]State Key Laboratory of Multiphase Flow in Power Engineering (SKLMF), Xi'an Jiaotong University, Xi'an, China

In the present study, the Fe-9Cr model alloy was irradiated with 240 keV He^{2+} at 550°C with a dose of 0.5 dpa at the peak damage region. The depth distribution of bubbles in Fe-9Cr alloy was investigated by transmission electron microscopy (TEM). The experimental results revealed that the spatial distribution of bubbles along the depth is different. In the region with higher helium concentration and irradiation dose, the bubbles inclined to be situated inside the plane of loops, forming a structure of "bubble-loop complex." However, in regions where the helium concentration and irradiation dose are relatively low, the number of "bubble-loop complexes" significantly decreased. In addition, the Burgers vector of "bubble-loop complexes" was identified as <100> type. Radiation-induced enrichment of Cr atoms at the "bubble-loop complexes" was also quantitatively estimated by energy-dispersive X-ray spectroscopy (EDS) in the scanning TEM mode.

Keywords: Fe-Cr alloys, bubble-loop complexes, He irradiation, Cr enrichment, dislocation loops

OPEN ACCESS

Edited by:
Wenzhong Zhou,
Sun Yat-Sen University, China

Reviewed by:
Fengfeng Luo,
Jiangxi Academy of Sciences, China
Xiang Zan,
Hefei University of Technology, China

****Correspondence:***
Di Yun
diyun1979@xjtu.edu.cn

Specialty section:
This article was submitted to Nuclear Energy, a section of the journal Frontiers in Energy Research

Received: *17 May 2021*
Accepted: *27 July 2021*
Published: *25 August 2021*

Citation:
Shi T, Liu W, Su Z, Yan X, Lu C, Yang Z, He X, Yan W and Yun D (2021) Formation of Bubble-Loop Complexes During Helium Radiation in Fe-9Cr Steel. Front. Energy Res. 9:710907. doi: 10.3389/fenrg.2021.710907

INTRODUCTION

The structural materials for the next generation fission reactors and fusion reactors will have to withstand high temperatures and a high neutron radiation dose (Zinkle and Was, 2013). In the reactor core materials, high-energy neutron irradiation will simultaneously cause Frenkel pairs and gas atoms such as helium (He) and hydrogen (H) (Marian et al., 2015). Different irradiation defects, such as nanoclusters, dislocation loops, and cavities, will be formed by the accumulation of Frenkel pairs and gas atoms. These irradiation defects will deteriorate the mechanical properties of structural materials by causing hardening, embrittlement, and swelling (Was, 2016).

Due to extremely low solubility and high mobility in the metal matrix, the behaviors of He atoms play a critical role in the microstructural evolution and mechanical properties of materials (Trinkaus and Singh, 2003; Samaras, 2009; Dai et al., 2012). The combination of He atoms with vacancies can cause the formation of stable helium-vacancy (He-Vac) clusters; these clusters can grow into bubbles or voids by absorbing He atoms and vacancies (Trinkaus and Singh, 2003). Besides, He atoms can be effectively trapped by the dislocations, grain boundaries (GBs), and precipitate-matrix interfaces that provide heterogeneous nucleation sites for the growth of bubbles or voids (Trinkaus and Singh, 2003). He atoms can also influence the loop microstructure (Arakawa et al., 2001; Lucas and Schäublin, 2008; Brimbal et al., 2014). The experiments of Brimbal et al. (2014) demonstrated that the simultaneous implantation of helium increased the number density and size of dislocation loops, which was attributed to two reasons. On the one hand, small He-Vac clusters can trap interstitial atoms (Arakawa

TABLE 1 | Concentrations of composition in Fe-9Cr alloy used in this study (wt%).

Alloy	Cr	C	N	O	P	S
Fe-9Cr	8.97	0.003	0.0014	0.013	0.0074	<0.003

et al., 2001) and the existence of helium favors the formation of interstitial clusters in displacement cascades (Lucas and Schäublin, 2008). On the other hand, He atoms can reduce the loops' mobility so that loops are left to absorb additional interstitials to further grow (Brimbal et al., 2014). Especially, it is also found that the He ion injection can lead to the heterogeneous nucleation of cavities or bubbles inside the plane of the dislocation loops in Fe-Cr alloys or ferritic-martensitic steels (Chen et al., 2008; Brimbal et al., 2011; Brimbal et al., 2014; Zhang et al., 2018; Bhattacharya et al., 2019; Li et al., 2020). This special structure between bubbles and loops was called "bubble-loop complexes" in some papers (Chen et al., 2008; Zhang et al., 2018; Li et al., 2020). Zhang et al. (2018) believed that this special structure can promote the growth of dislocation loops. However, the formation mechanism and conditions of this structure are still unclear.

Apart from causing various defects in materials, irradiation can also lead to radiation-induced segregation/precipitation (RIS/RIP) at sinks such as GBs, precipitate/matrix interfaces (Jiao and Was, 2011), which may reduce the oxidation or corrosion resistance of materials (Was, 2016). In addition, RIS also occurs in the vicinity of radiation-induced defects such as dislocation loops (Yoshida et al., 1988; Neklyudov and Voyevodin, 1994; Jiao and Was, 2011; Bhattacharya et al., 2014). For instance, the Cr atoms can enrich on dislocation loops during the process of irradiation (Yoshida et al., 1988; Neklyudov and Voyevodin, 1994; Bhattacharya et al., 2014), which can suppress the motion of the loops (Arakawa et al., 2004; Terentyev et al., 2013).

Currently, ferritic-martensitic steels are candidate structural materials for the generation-IV fission reactors and fusion reactors (Yvon and Carré, 2009) owing to their higher swelling resistance as compared to austenitic steels (Blasl et al., 1985; Klueh and Harries, 2001). Fe-Cr alloys, as the model steels, have been used to study the basic irradiation damage mechanisms of complex ferritic-martensitic steels. In order to study the helium behavior in Fe-Cr alloys, the bulk specimen of a Fe-9Cr model alloy was irradiated with 240 keV He^{2+} at 550°C in this study. The depth distribution of radiation-induced defects in Fe-9Cr alloy irradiated by He ions was investigated by transmission electron microscopy (TEM) and scanning transmission electron microscope (STEM). The "bubble-loop complexes" were observed and characterized in detail. In addition, the Cr enrichment at "bubble-loop complexes" was also analyzed by energy-dispersive X-ray spectroscopy (EDS) measurements in the STEM mode.

MATERIALS AND EXPERIMENTAL PROCEDURE

The Fe-9Cr model alloy used in this work was melted into an ingot in a vacuum induction furnace, and then the ingot was forged and hot-rolled to a 12 mm thick plate. The chemical compositions of the material are listed in **Table 1**. Before radiation, the material was heat-treated at 920°C for 30 min followed by air cooling and then tempered at 720°C for 1 h. The preparation process of the metallographic sample is as follows: the bulk specimen was mechanically polished using SiC abrasives from 400 grit up to 2000 grit and the diamond polishing fluids with particles of 0.3 μm, and then the sample surface was etched with an etching solution of 5 ml hydrochloric acid and 1 g picric acid in 100 ml ethanol. Optical Microscopy (OM) observation showed that the initial microstructure of the material is all ferrite and the average grain size is about 75 μm. A bulk sample with a dimension of 9 mm × 6 mm × 2 mm for irradiation experiment was cut from the heat-treated steel plate by spark erosion, and then it was mechanically polished. Finally, the surface of the specimen was electrolytically polished in an electrolyte of 10% perchloric acid in ethanol.

The irradiation experiment was performed at the 320 kV platform for multidiscipline research with highly charged ions at the Institute of Modern Physics (IMP), Chinese Academy of Sciences. The specimen of Fe-9Cr model alloy was irradiated with 240 keV He^{2+} at 550°C to a dose of 0.5 dpa at the peak damage region. The dose rate was 1.4×10^{-4} dpa/s and the influence of ions was 2.1×10^{16} cm^{-2}. The displacement damage, helium content, and the He/dpa ratio (appm/dpa) were calculated by using the "Quick Calculation (K-P)" mode in SRIM 2013 and the displacement energy of 40 eV was used for Fe-9Cr alloy (Was, 2016). A typical damage profile across the Fe-9Cr sample depth is illustrated in **Figure 1**.

TEM foil samples for microstructure characterization were prepared using a focused ion beam (FIB) system. Flash polishing was used to remove the FIB damage caused by the FIB lift-out process. The process of flash polishing is as follows (Lu et al., 2016). An electropolishing apparatus with an electrolytic solution of 5% perchloric acid in 95% ethanol was used to do flash polishing. The electric potential applied to the FIB-polished

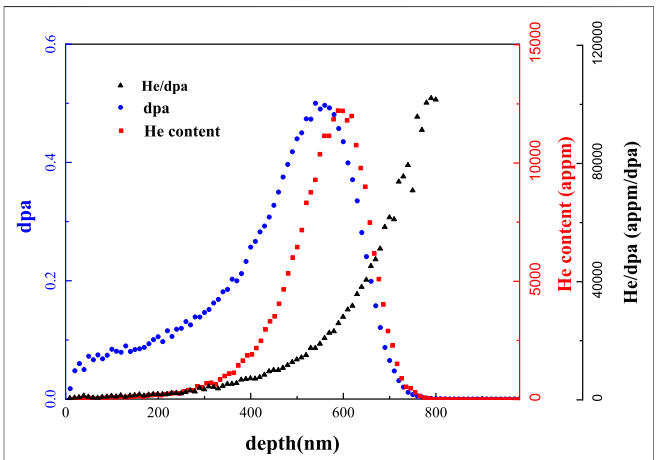

FIGURE 1 | The profile of dpa, He content, and the He/dpa ratio calculated for Fe-9Cr alloy irradiated with 240 keV He^{2+} ion by using SRIM 2013.

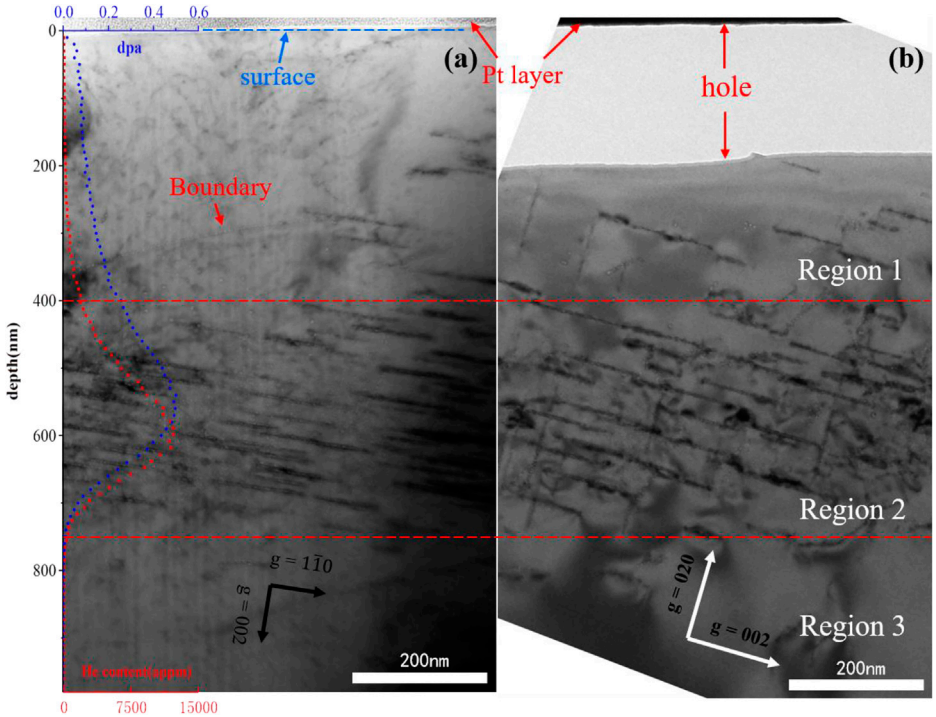

FIGURE 2 | TEM bright-field (BF) images showing the spatial distribution of bubbles of Fe-9Cr alloy **(A)** under <110> zone axis and **(B)** under <100> zone axis.

specimen was 6–14 V and the temperature range was between −30 and −50°C. An accurate timer was used to control the time of flash polishing between 0.05 and 0.2 s. The final thickness of the FIB sample is about 70 nm. The under-focus condition in a JEOL JEM-F200 TEM microscope was used to image He bubbles. The dislocation loops were imaged on the zone axis under the STEM mode in a Talos F200X microscope. Details about the conditions and methods of dislocation loop imaging in the STEM mode can be found in Parish et al. (2015). STEM-EDS technique was conducted to characterize the compositional distribution in Fe-9Cr alloy. The standard deviation of the size measurement data was used to calculate the size error and the standard deviation of the density of three to four different regions was used to calculate the density error.

RESULTS AND DISCUSSION

Bubble Spatial Distribution in Irradiated Fe-9Cr Alloy

Figures 2A,B show, respectively, the cross-sectional TEM bright-field (BF) images taken under <110> and <100> zone axes of Fe-9Cr alloy irradiated by 240 keV helium ions. The FIB sample shown in **Figure 2B** was processed by flash polishing and the region between the surface and 200 nm depth in this sample was corroded away by the electrolytic solution, so there existed an elongated hole with a width of about 200 nm below the platinum layer. In order to obtain the information of bubbles in the region between surface and 200 nm depth, a whole FIB sample without processing by flash polishing is shown in **Figure 2A**. The start points in **Figures 2A,B** are all the bottom surfaces of the platinum layer. It was found that the spatial distribution of bubbles is different along with the depth in **Figure 2**. According to the characteristic of bubble distribution, the irradiation damage region was divided into three regions. In region 1 (from the surface to 400 nm depth), the small He bubbles were distributed in the matrix and on GBs and a few linear arrangements of bubbles were also observed in the range between 200 and 400 nm depth. The reason for linear arrangements of bubbles is that some bubbles were located inside loops that are edge-on. As mentioned in the introduction, these peculiar structures combining bubbles and loops were commonly referred to as "bubble-loop complexes." In region 2 (between the depth of 400 and 750 nm), the obvious feature of the spatial distribution of bubbles is that a large number of bubble-loop complexes appeared in this region. Region3, which is beyond the damage region calculated by SRIM, is between the depth of 750 and 900 nm. In this region, most bubbles precipitated on preexisting dislocation lines or GBs and no bubble-loop complexes were observed. The images of bubbles detected in these three different regions are shown in **Figure 3**.

According to the He content distribution calculated by SRIM, there exists a difference in the He content along with the depth, so it can be inferred that the variance of bubble spatial distribution along the depth is related to the difference of the He content in different regions. The TEM-BF images taken under <110> zone axis were used to measure the bubble size and density in different three regions and the statistical results are shown in **Table 2**.

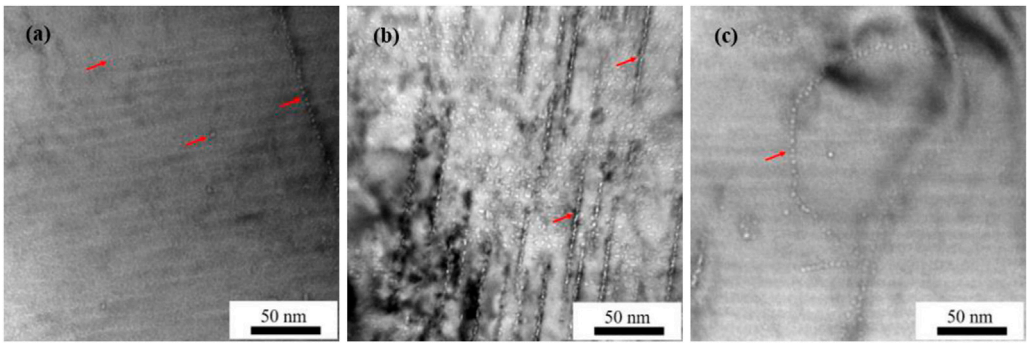

FIGURE 3 | TEM BF images taken under <110> zone axis showing the bubble distribution in different regions: **(A)** in region 1, the red arrows indicate small bubbles at the matrix and on the GBs, **(B)** in region 2, the red arrows indicate bubbles inside the plane of loops, and **(C)** in region 3, the red arrows indicate bubbles at the dislocation lines.

TABLE 2 | Summary of average size and density of bubbles in different regions.

	Average size (nm) (number of bubbles measured)	Average density ($\times 10^{22}$ m^{-3})
Region 1	2.4 ± 0.9 (58)	2.2 ± 0.5
Region 2	2.7 ± 1.2 (70)	11.6 ± 3.3
Region 3	2.2 ± 0.4 (62)	2.1 ± 0.9

Figure 4 shows the average size and density of bubbles in different three regions. It was found that the average bubble size changes little along with the depth, but the bubble number density in the helium-rich region (region 2) is higher than that in the helium-depleted regions (region 1 and region 3).

Bubble-Loop Complexes

Figure 5 shows the TEM-BF images showing the structure of bubble-loop complexes taken under <100>, <110>, and <111> zone axes. Different morphologies of "bubble-loop complexes" in region 2 were displayed under three different zone axes. As mentioned above, the linear arrangements of bubbles in these images correspond to the "bubble-loop complexes" where the loops are edge-on. The linear arrangements of bubbles were not observed in the <111> zone axis since no loops are edge-on in the <111> zone axis, which has been demonstrated by the dislocation loops orientation maps developed by Yao et al. for bcc Fe-based materials (Yao et al., 2013). **Figure 6** shows STEM-BF images taken near <100>, <110>, and <111> zone axes, and the structure of "bubble-loop complexes" can be observed more clearly in the STEM-BF mode. In addition, combining the STEM-BF images and the dislocation loop orientation maps developed by Yao et al. (2013) (as shown in **Figure 6**), the Burgers vector of the loops in the "bubble-loop complexes" was identified as <100>. This is consistent with the findings of many irradiation experiments in which only <100> loops existed above 500 °C in Fe-Cr alloys or F/M steels (Jenkins et al., 2009; Liu et al., 2017). The size distribution of bubble-loop complexes in irradiated Fe-9Cr alloy is shown in **Figure 7**. **Figure 8** shows the cross-sectional

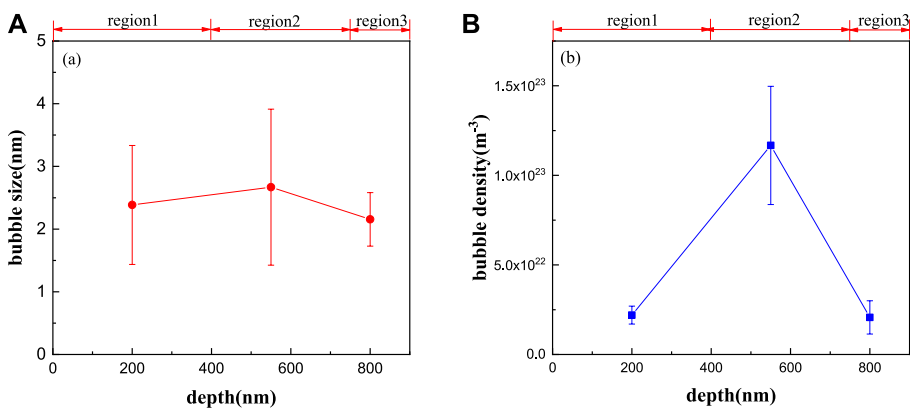

FIGURE 4 | (A) The average size of bubbles in different depth ranges and **(B)** the average density of bubbles in different depth ranges.

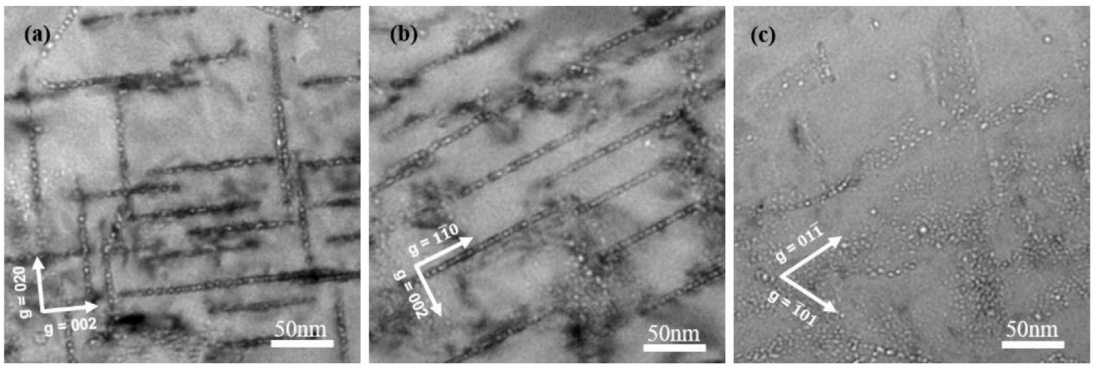

FIGURE 5 | TEM BF images showing the structure of bubble-loop complexes: **(A)** under <100> zone axis, **(B)** under <110> zone axis, and **(C)** under <111> zone axis.

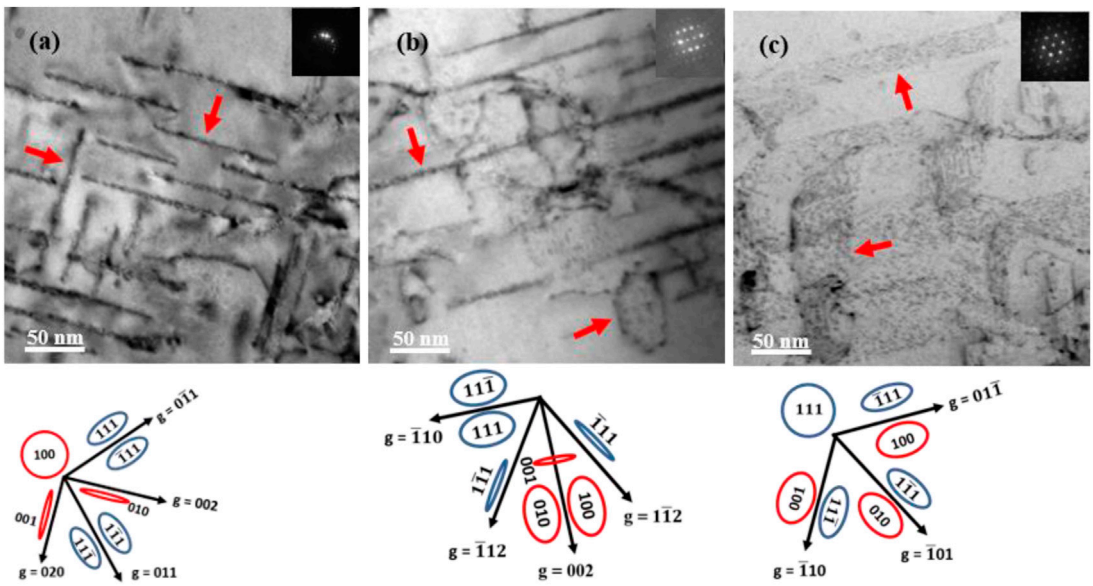

FIGURE 6 | STEM BF images showing bubble-loop complexes: **(A)** under <100> zone axis, **(B)** under <110> zone axis, and **(C)** under <111> zone axis; the red arrows indicate bubble-loop complexes.

STEM-BF image taken under <100> zone axis at low magnification. Although there were some bubble-loop complexes in the region between 200 and 400 nm, most of them were mainly distributed in region 2. In region 3, no bubble-loop complexes were found. The STEM-BF images taken under <100> zone axis were used to measure the size and density of bubble-loop complexes in region 1 and region 2. The statistical results are shown in **Table 3**. The density of bubble-loop complexes in region 2 is about three times as large as that in region 1, which is consistent with the trend of change of bubble density along with the depth.

Bubble-loop complexes have been observed in pure Fe and Fe-Cr-based steels irradiated by dual-beam ions (Fe ion + He ion) and single-beam He ions (Brimbal et al., 2014; Chen et al., 2008; Brimbal et al., 2011; Bhattacharya et al., 2019; Zhang et al., 2018; Li et al., 2020). Chen et al. (2008) found the bubble-loop complexes in oxide dispersion strengthened (ODS) ferritic steel PM2000 irradiated by He ions at 400 °C. Brimbal et al. (2011); Brimbal et al. (2014) identified bubble-loop complexes in α-Fe irradiated by He and Fe dual-beam ions at 500°C. Bhattacharya et al. (2019) observed heterogeneous cavity nucleation inside dislocation loops in Fe-Cr alloys irradiated by Fe and He dual-beam ions at 500°C. Recently, Li et al. (2020) systematically investigated the behaviors of bubble-loop complexes in He-irradiated CLAM steels at different temperatures. Their research showed that bubble-loop complexes appeared when the samples were irradiated at the temperature of 250°C and above. The irradiation conditions of the above experiments and this study where the bubble-loop complexes were observed are summarized in **Table 4**. The dpa shown in **Table 4** was

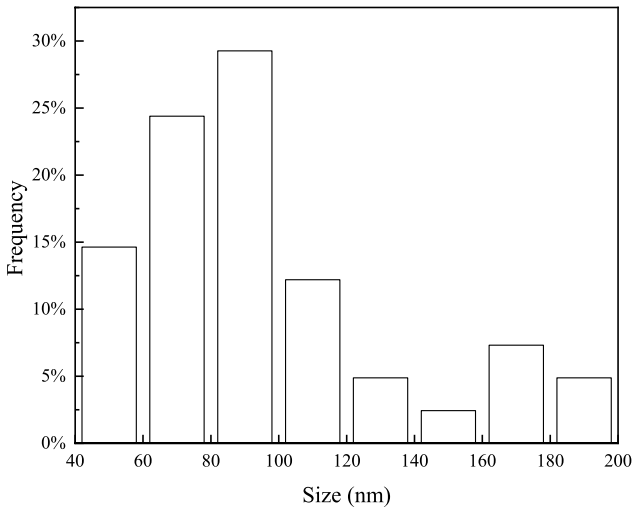

FIGURE 7 | Size distribution of bubble-loop complexes in irradiated Fe-9Cr alloy.

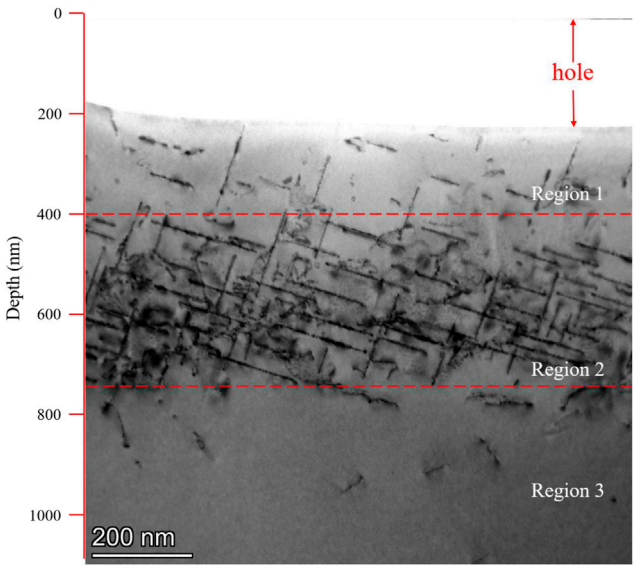

FIGURE 8 | STEM BF images showing the spatial distribution of loops of Fe-9Cr alloy near <100> zone axis.

TABLE 3 | Summary of average size and density of bubble-loop complexes in different regions.

	Average size (nm) (number of bubble-loop complexes measured)	Average density ($\times 10^{20}$ m^{-3})
Region 1	89.0 ± 37.5 (19)	9.8 ± 0.6
Region 2	94.6 ± 38.0 (41)	29.7 ± 2.3
Region 3	Not found	Not found

Not found: bubble-loop complexes were not found in region 3.

converted to the numerical value of dpa in the "Quick Calculation (K-P)" mode. As can be seen from **Table 4**, bubble-loop complexes usually appeared under irradiation conditions with relatively high temperatures. The experiment results of Li et al. (2020) also indicated that bubble-loop complexes were easily formed at a high temperature. Besides, a high He/dpa ratio is also believed to contribute to the formation of bubble-loop complexes. However, Bhattacharya et al. (2019) also observed these structures under the irradiation condition with a low He/dpa ratio (~20). Their experimental results showed that bubble-loop complexes appeared beyond the damage peak, and they believed that the existence of a different dislocation loop microstructure in front of and beyond the damage peak and the high concentration of He around the damage peak resulted in the formation of this peculiar structure. In our study, bubble-loop complexes mainly were distributed in region 2 where the He concentration is relatively higher. In addition, the irradiation dose in region 2 is also higher than that in region 1 and region 3, which can cause the formation of a different loop structure in region 2 compared to the other two regions. Therefore, a relatively high He content and a radiation dose prompted the formation of bubble-loop complexes in region 2.

A possible mechanism was formulated by Brimbal et al. (2011) to explain the formation of bubble-loop complexes. There exists positive binding energy between helium with <111> type dislocations (Heinisch et al., 2006; Yang et al., 2007; Heinisch et al., 2010) and <111> type dislocation loops (Shim et al., 2007), and He atoms can be trapped at the dislocation core. The mobility of the trapped helium atoms by "pipe-diffusion" in the dislocation core can cause the nucleation of small helium clusters. These clusters are left behind in their as-nucleated locations when the dislocation loops grow larger by preferential absorption of interstitials. Because He atoms are insoluble in the Fe matrix, these clusters are stable and can grow by further absorbing He atoms or vacancies until they are observed in TEM as bubbles inside the loop plane. Based on the atomistic simulations (Yang et al., 2013; Li et al., 2020), a different mechanism was proposed by Li et al. (2020). In the process of He^+ irradiation, the self-interstitial atoms (SIAs) are attached to the He-Vac clusters to form the initial He-Vac-SIA complexes. These He-Vac-SIA complexes can further absorb SIA clusters and/or He-Vac clusters and grow up into the bubble-loop complexes observed in TEM at relatively high temperatures. The difference between the two mechanisms is that one believes that the formation of bubble-loop complexes was originated from the interaction between dislocation loops and He atoms while the other believes that bubble-loop complexes were formed by direct nucleation and growth of He-Vac-SIA complexes. If the mechanism proposed by Li et al. (2020) was operating in our experiment, the nucleation of the He-Vac-SIA complexes should have been homogeneous in region 1, and the homogeneous nucleated He-Vac-SIA complexes should have been able to further absorb irradiation-induced interstitial clusters, He atoms, and vacancies in a uniform manner. As a result, the expected distribution of bubble-loop complexes would be uniformly distributed complexes with a smaller size than those in region 2 since the irradiation-

TABLE 4 | Summary of experimental studies on bubble-loop complexes in bcc Fe (Cr) alloys and F/M steels. T: irradiation temperature.

Materials	Irradiation	T (°C)	He content (appm)	dpa	He/dpa (appm/dpa)	Burgers vector	Loop size (nm)	Loop density ($\times 10^{21}$ m^{-3})	Ref
ODS ferritic steel bulk	He^+	400	3,000	0.38	7,890	<100> and <111>	56	3.21	Chen et al. (2008)
Fe thin foil	He^+ and Fe^+	500	540	0.45	1,200	<100>	75	0.73	Brimbal et al. (2011)
Fe thin foil	He^+ and Fe^+	500	63 540	0.4 0.4	158 1,350	<100> and <111> <100>	Not measured 85	Not measured 0.61	Brimbal et al. (2014)
Fe-Cr bulk (3%-14 wt% Cr)	He^+ and Fe^+	500	2,980	134	20	Not measured	Not measured	Not measured	Bhattacharya et al. (2019)
CLAM steel foil	He^+	250 350 400 450 550	~10,000	0.37	27,027	<100> and <111> <100> and <111> <100> <100> <100>	3.72 7.96 23.25 51.32 29.25	55.8 23.4 11.8 1.71 4.86	Li et al. (2020)
Fe-9Cr bulk	He^+	550	~10,370	0.5	20,740	<100>	94.6	2.97	This study

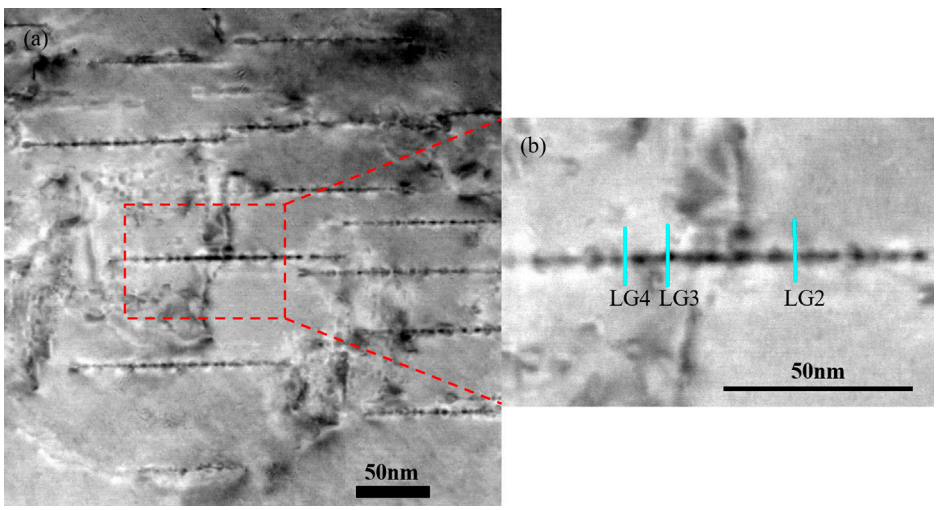

FIGURE 9 | The high-angle annular dark-field (HAADF) image of bubble-loop complexes taken on <110> zone axis; the blue lines represent the traces of the line scan for EDS measurement.

supplied interstitials, He atoms, and vacancies in region 1 would have been more dispersedly partitioned into each bubble-loop complex. This, however, was not the situation observed in region 1 in our experiment. Our experimental results indicated that the size of bubble-loop complexes in region 1 is similar to that in region 2. Thus, the mechanism proposed by Li et al. (2020) may not explain the formation of bubble-loop complexes, and the mechanism proposed by Brimbal et al. (2011) is believed to better explain the difference in the distribution of bubble-loop complexes in our experiment. In region 2, the irradiation dose and He content are relatively high, and more interstitial clusters were formed in this region. When the small interstitial clusters grew to dislocation loops of a certain size, the core of loops trapped the He atoms in the matrix. These trapped He atoms evolved into small helium clusters or He-Vac clusters at the core of loops and pinned the dislocation loops. Then these immobile loops, like sinks, continued to grow by absorption of interstitial atoms. Simultaneously, these small helium clusters or He-Vac clusters at the core of loops were left inside the loop plane and grew into bubbles by absorbing He atoms or vacancies, forming a large number of bubble-loop complexes in region 2 eventually. Since the irradiation dose in region 1 is lower than that in region 2, the number of initial dislocation loops formed in region 1 is less than that in region 2, resulting in fewer bubble-loop complexes formed in region 1. In addition, the similar size of the bubble-loop complexes in region 1 as compared to those in region 2 gives us a reason to believe that these complexes in both regions experienced similar growth kinetics (as the number density of bubble-

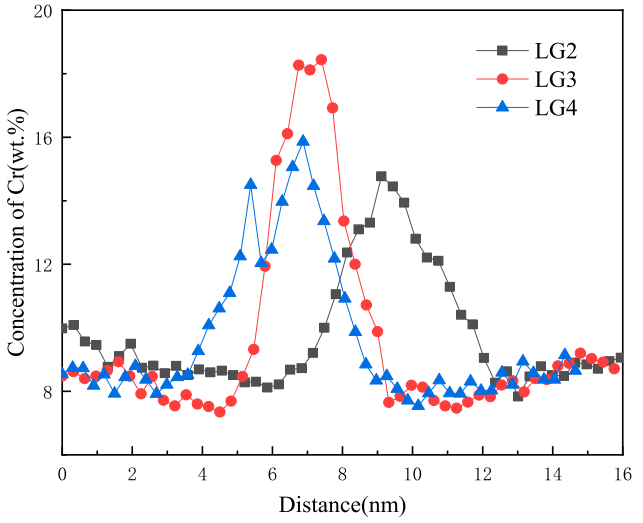

FIGURE 10 | Concentration profiles of Cr at the bubble-loop complexes obtained by EDS analysis.

loop complexes and He content are nearly proportionally distributed between region 1 and region 2). In region 3, the irradiation dose decreased to zero. There were not enough SIAs to form visible loops and helium in the matrix would not be trapped by the loops. Therefore, no bubble-loop complexes were observed in region 3.

Cr Segregation on the Bubble-Loop Complexes

STEM-EDS measurements were performed on the bubble-loop complexes. The measurement method is the same as that used by Bhattacharya (Bhattacharya et al., 2014). For reliable estimates by EDS on dislocation loops, it is essential that the normal of the two-dimensional planes should be exactly vertical to the electron beam direction. Thus, the FIB sample was tilted to [110] zone axis. When the electron beam was aligned with the [110] zone axis, <001>-type dislocation loop families were perfectly on edge in our study. **Figure 9** shows the high-angle annular dark-field (HAADF) image taken on <110> zone axis of the FIB sample. The black lines shown in **Figure 9A** correspond to bubble-loop complexes which are edge-on. **Figure 9B** shows three line scans in one bubble-loop complex and each line scan contained 50 points. The results of the line scans are plotted in **Figure 10**; it should be noted that the center point of LG2 was above in the black line representing the bubble-loop complex, so the peak of LG2 is the right side of the peak of LG3 and LG4 in **Figure 10**. The measurement results are believed to represent the Cr enrichment in the bubble-loop complexes. In addition, the results of the line scans also revealed that the values of Cr enrichment in different locations of an edge-on bubble-loop complex are different, which demonstrated that the Cr enrichment was heterogeneous. This is consistent with the experimental results of Bhattacharya et al. (2014) as well. A total of 20 line scans were done and the average peak value of Cr enrichment is about 18.86 ± 3.07 wt%. The behavior of Cr enrichment at the bubble-loop complexes is similar to that of Cr enrichment at dislocation loops. The phenomenon of the segregation of Cr at dislocation loops has been reported by many researchers (Jiao and Was, 2011; Neklyudov and Voyevodin, 1994; Yoshida et al., 1988; Bhattacharya et al., 2014). For instance, Neklyudov and Voyevodin (1994) observed the enrichment of Cr and Si at dislocation loops in 13Cr2MoNb-VB steel irradiated with chromium ions to 48 dpa at 575°C. Yoshida et al. (1988) discovered the enrichment of Cr and Ni at dislocation loops in high-purity Fe-10Cr and Fe-10Cr-1Ni alloys irradiated by electrons. Bhattacharya et al. (2014) reported the Cr enrichment at dislocation loops in ion-irradiated high-purity Fe-11Cr alloys at 500°C. The Cr depletion at dislocation loops was also reported in HCM12A steel after ion irradiation at 400°C by Jiao and Was (2011). **Table 5** summarizes the segregation behaviors of Cr at

TABLE 5 | Summary of segregation of Cr at dislocation loops in literature and this study.

Material	Radiation type	Temperature (°C)	Dose (dpa)	Dose rate (dpa/s)	Analysis method	Depletion or enrichment	The Cr content measured on loops	Difference of Cr content between matrix and loops	Ref
HCM12A	Proton	400	7	~10–5	APT	Depletion	~10 at%	~ -1.6 at%	Jiao and Was (2011)
13Cr2MoNb-VB	Ion (Cr^{3+})	575	48	~10–1	TEM-EDS	Enrichment	~14 wt%	~1 wt%	Neklyudov and Voyevodin (1994)
Fe-10Cr	Electron	500	0.35	/	TEM-EDS	Enrichment	~12 wt%	~2 wt%	Yoshida et al. (1988)
Fe-10Cr-1Ni	Electron	500	0.35	/	TEM-EDS	Enrichment	~11 wt%	~1 wt%	Yoshida et al. (1988)
Fe-11Cr	Ion (Fe^{3+}+He^{+})	500	45	~10–4	TEM-EDS /APT	Enrichment	22–33 wt% 21 wt% (APT)	11–22 wt% 10 wt% (APT)	Bhattacharya et al. (2014)
Fe-9Cr	Ion (He^{2+})	550	0.5	~10–4	TEM-EDS	Enrichment	~19 wt%	~10 wt%	This study

dislocation loops in the above literature and this study. The values of Cr enrichment in experiments of Bhattacharya et al. (2014) and this study are larger than those measured in other experiments. In irradiation experiments of Bhattacharya et al. (2014) and ours, the helium ions were injected into irradiation materials. Hence, helium atoms in irradiation materials possibly promoted the enrichment of Cr at dislocation loops. But Bhattacharya et al. (2014) believed that the effect of helium on the enrichment of Cr at dislocation loops is limited. Because the compositions of irradiation materials and irradiation conditions in the above experiments are different, the direct comparison of values of Cr enrichment in these experiments may be unreliable. The effect of helium on the Cr enrichment at dislocation loops needs further systematic studies.

CONCLUSION

In this study, the Fe-9Cr model alloy was irradiated with He^{2+} up to 0.5 dpa peak dose at 550°C. The microstructure after irradiation was investigated by TEM and STEM. The experimental results indicated that the spatial distribution of He bubbles is different along with the depth. In the region with higher He concentration and irradiation dose, a large number of bubble-loop complexes (bubbles inside loops) were formed. But in some regions with lower He concentration and irradiation dose, the number of bubble-loop complexes decreased significantly or these structures even were not observed. It is believed, based on our experimental observations, that the mechanism proposed by Brimbal et al. can better explain the formation mechanism of the bubble-loop complexes. The Burgers vector of "bubble-loop complexes" was identified as <100> type. In addition, the Cr enrichment at the bubble-loop complexes was also quantitatively estimated by STEM-EDS measurements and the average peak value of Cr enrichment is 18.86 ± 3.07 wt%.

DATA AVAILABILITY STATEMENT

The raw data supporting the conclusions of this article will be made available by the authors, without undue reservation.

AUTHOR CONTRIBUTIONS

TS: conceptualization, methodology, investigation, writing—original draft. WL: methodology and investigation. ZS: investigation. XY: investigation. CL: conceptualization, methodology, and writing—review and editing. ZY: investigation. XH: conceptualization, methodology, and writing—review and editing. WY: material preparation. DY: conceptualization, writing—review and editing, and funding acquisition.

FUNDING

Financial support provided by the National Natural Science Foundation of China (No. 11705137), NSAF Joint Fund (No. U1830124), and China Postdoctoral Science Foundation (No. 2018T111053) is acknowledged. The authors thank Dr. Chao Li and Dr. Jiao Li at Instrument Analysis Center of Xi'an Jiaotong University for their assistance with TEM and STEM analysis.

REFERENCES

Arakawa, K., Hatanaka, M., Mori, H., and Ono, K. (2004). Effects of Chromium on the One-Dimensional Motion of Interstitial-type Dislocation Loops in Iron. *J. Nucl. Mater.* 329-333, 1194–1198. doi:10.1016/j.jnucmat.2004.04.263

Arakawa, K., Imamura, R., Ohota, K., and Ono, K. (2001). Evolution of point Defect Clusters in Pure Iron under Low-Energy He+ Irradiation. *J. Appl. Phys.* 89, 4752–4757. doi:10.1063/1.1357785

Bhattacharya, A., Meslin, E., Henry, J., Leprêtre, F., Décamps, B., and Barbu, A. (2019). Combined Effect of Injected Interstitials and He Implantation, and Cavities inside Dislocation Loops in High Purity Fe-Cr Alloys. *J. Nucl. Mater.* 519, 30–44. doi:10.1016/j.jnucmat.2019.03.043

Bhattacharya, A., Meslin, E., Henry, J., Pareige, C., Décamps, B., Genevois, C., et al. (2014). Chromium Enrichment on the Habit Plane of Dislocation Loops in Ion-Irradiated High-Purity Fe-Cr Alloys. *Acta Materialia* 78, 394–403. doi:10.1016/j.actamat.2014.06.050

Blasl, D., Tsunakawa, H., Miyahara, K., and Igata, N. (1985). Void Swelling and Microstructure Evolution of a Dual Phase (Ferritic and Austenitic) Stainless Steel. *J. Nucl. Mater.* 133-134, 517–520. doi:10.1016/0022-3115(85)90201-6

Brimbal, D., Décamps, B., Barbu, A., Meslin, E., and Henry, J. (2011). Dual-beam Irradiation of α-iron: Heterogeneous Bubble Formation on Dislocation Loops. *J. Nucl. Mater.* 418, 313–315. doi:10.1016/j.jnucmat.2011.06.048

Brimbal, D., Décamps, B., Henry, J., Meslin, E., and Barbu, A. (2014). Single- and Dual-Beam *In Situ* Irradiations of High-Purity Iron in a Transmission Electron Microscope: Effects of Heavy Ion Irradiation and Helium Injection. *Acta Materialia* 64, 391–401. doi:10.1016/j.actamat.2013.10.052

Chen, J., Jung, P., Hoffelner, W., and Ullmaier, H. (2008). Dislocation Loops and Bubbles in Oxide Dispersion Strengthened Ferritic Steel after Helium Implantation under Stress. *Acta Materialia* 56, 250–258. doi:10.1016/j.actamat.2007.09.016

Dai, Y., Odette, G. R., and Yamamoto, T. (2012). The Effects of Helium in Irradiated Structural Alloys. *Compr. Nucl. Mater.* 1, 141–193. doi:10.1016/b978-0-08-056033-5.00006-9

Heinisch, H. L., Gao, F., and Kurtz, R. J. (2010). Atomic-scale Modeling of Interactions of Helium, Vacancies and Helium-Vacancy Clusters with Screw Dislocations in Alpha-Iron. *Phil. Mag.* 90, 885–895. doi:10.1080/14786430903294932

Heinisch, H. L., Gao, F., Kurtz, R. J., and Le, E. A. (2006). Interaction of Helium Atoms with Edge Dislocations in α-Fe. *J. Nucl. Mater.* 351, 141–148. doi:10.1016/j.jnucmat.2006.02.027

Jenkins, M. L., Yao, Z., Hernández-Mayoral, M., and Kirk, M. A. (2009). Dynamic Observations of Heavy-Ion Damage in Fe and Fe-Cr Alloys. *J. Nucl. Mater.* 389, 197–202. doi:10.1016/j.jnucmat.2009.02.003

Jiao, Z., and Was, G. S. (2011). Segregation Behavior in Proton- and Heavy-Ion-Irradiated Ferritic-Martensitic Alloys. *Acta Materialia* 59, 4467–4481. doi:10.1016/j.actamat.2011.03.070

Klueh, R. L., and Harries, D. R. (2001). *High-Chromium Ferritic and Martensitic Steels for Nuclear Applications*. West Conshohocken, PA: ASTM.

Li, F., Wei, Y., Luo, F., Zhang, W., Zhou, X., Chen, Y., et al. (2020). Behaviors of Bubble-Loop Complexes in He-Irradiated CLAM Steels at Elevated Temperatures. *J. Nucl. Mater.* 529, 151954. doi:10.1016/j.jnucmat.2019.151954

Liu, X., Miao, Y., Li, M., Kirk, M. A., Maloy, S. A., and Stubbins, J. F. (2017). Ion-irradiation-induced Microstructural Modifications in Ferritic/martensitic Steel T91. *J. Nucl. Mater.* 490, 305–316. doi:10.1016/j.jnucmat.2017.04.047

Lu, C., Jin, K., Béland, L. K., Zhang, F., Yang, T., Qiao, L., et al. (2016). Direct Observation of Defect Range and Evolution in Ion-Irradiated Single Crystalline Ni and Ni Binary Alloys. *Sci. Rep.* 6, 1–10. doi:10.1038/srep19994

Lucas, G., and Schäublin, R. (2008). Helium Effects on Displacement Cascades in α-iron. *J. Phys. Condens. Matter* 20, 415206. doi:10.1088/0953-8984/20/41/415206

Marian, J., Hoang, T., Fluss, M., and Hsiung, L. L. (2015). A Review of Helium-Hydrogen Synergistic Effects in Radiation Damage Observed in Fusion Energy Steels and an Interaction Model to Guide Future Understanding. *J. Nucl. Mater.* 462, 409–421. doi:10.1016/j.jnucmat.2014.12.046

Neklyudov, I. M., and Voyevodin, V. N. (1994). Features of Structure-phase Transformations and Segregation Processes under Irradiation of Austenitic and Ferritic-Martensitic Steels. *J. Nucl. Mater.* 212-215, 39–44. doi:10.1016/0022-3115(94)90031-0

Parish, C. M., Field, K. G., Certain, A. G., and Wharry, J. P. (2015). Application of STEM Characterization for Investigating Radiation Effects in BCC Fe-Based Alloys. *J. Mater. Res.* 30, 1275–1289. doi:10.1557/jmr.2015.32

Samaras, M. (2009). Multiscale Modelling: the Role of Helium in Iron. *Mater. Today* 12, 46–53. doi:10.1016/S1369-7021(09)70298-6

Shim, J.-H., Kwon, S. C., Kim, W. W., and Wirth, B. D. (2007). Atomistic Modeling of the Interaction between Self-Interstitial Dislocation Loops and He in Bcc Fe. *J. Nucl. Mater.* 367-370, 292–297. doi:10.1016/j.jnucmat.2007.03.005

Terentyev, D., Bergner, F., and Osetsky, Y. (2013). Cr Segregation on Dislocation Loops Enhances Hardening in Ferritic Fe-Cr Alloys. *Acta Materialia* 61, 1444–1453. doi:10.1016/j.actamat.2012.11.021

Trinkaus, H., and Singh, B. N. (2003). Helium Accumulation in Metals during Irradiation - where Do We Stand? *J. Nucl. Mater.* 323, 229–242. doi:10.1016/j.jnucmat.2003.09.001

Was, G. S. (2016). *Fundamentals of Radiation Materials Science: Metals and Alloys*. New York: Springer.

Yang, L., Deng, H. Q., Gao, F., Heinisch, H. L., Kurtz, R. J., Hu, S. Y., et al. (2013). Atomistic Studies of Nucleation of He Clusters and Bubbles in Bcc Iron. *Nucl. Instr. Methods Phys. Res. Section B: Beam Interactions Mater. Atoms* 303, 68–71. doi:10.1016/j.nimb.2012.11.025

Yang, L., Zu, X. T., Wang, Z. G., Gao, F., Wang, X. Y., Heinisch, H. L., et al. (2007). Interaction of Helium-Vacancy Clusters with Edge Dislocations in α-Fe. *Nucl. Instr. Methods Phys. Res. Section B: Beam Interactions Mater. Atoms* 265, 541–546. doi:10.1016/j.nimb.2007.10.007

Yao, B., Edwards, D. J., and Kurtz, R. J. (2013). TEM Characterization of Dislocation Loops in Irradiated Bcc Fe-Based Steels. *J. Nucl. Mater.* 434, 402–410. doi:10.1016/j.jnucmat.2012.12.002

Yoshida, N., Yamaguchi, A., Muroga, T., Miyamoto, Y., and Kitajima, K. (1988). Characteristics of point Defects and Their Clustering in Pure Ferritic Steels. *J. Nucl. Mater.* 155-157, 1232–1236. doi:10.1016/0022-3115(88)90502-8

Yvon, P., and Carré, F. (2009). Structural Materials Challenges for Advanced Reactor Systems. *J. Nucl. Mater.* 385, 217–222. doi:10.1016/j.jnucmat.2008.11.026

Zhang, W., Shen, Z., Long, Y., Wei, Y., Zhou, X., Chen, C., et al. (2018). Bubble-loop Complexes Induced by Helium Irradiation and Effect of Pre-irradiation and post-irradiation of Hydrogen in Reduced-Activation Ferritic/martensitic Steel. *Phil. Mag.* 98, 2495–2511. doi:10.1080/14786435.2018.1492159

Zinkle, S. J., and Was, G. S. (2013). Materials Challenges in Nuclear Energy. *Acta Materialia* 61, 735–758. doi:10.1016/j.actamat.2012.11.004

Conflict of Interest: The authors declare that the research was conducted in the absence of any commercial or financial relationships that could be construed as a potential conflict of interest.